Supporting information for:

3D Lead-Organoselenide-Halide Perovskites and their Mixed-Chalcogenide and Mixed-Halide Alloys

Jiayi Li,[a] Yang Wang,[b] Santanu Saha,[c,d] Zhihengyu Chen,[e] Jan Hofmann,[e] Jason Misleh,[a] Karena W. Chapman,[e] Jeffrey A. Reimer,[b,f] Marina R. Filip,[*,c] and Hemamala I. Karunadasa[*,a,g]

[a]*Department of Chemistry, Stanford University, Stanford, California 94305, United States*

[b]*Department of Chemical and Biomolecular Engineering, College of Chemistry, UC Berkeley, Berkeley, California 94720, United States*

[c]*Department of Physics, University of Oxford, Clarendon Laboratory, Parks Road, Oxford OX1 3PU, United Kingdom*

[d]*Institut de Recherche sur les Ceramiques (IRCER), UMR CNRS 7315-Université de Limoges, 12 Rue Atlantis, Limoges 87068, France*

[e]*Department of Chemistry, Stony Brook University, Stony Brook, New York 11794, United States*

[f]*Materials Sciences Division, Lawrence Berkeley National Laboratory, Berkeley, California 94720, United States*

[g]*Stanford Institute for Materials and Energy Sciences (SIMES), SLAC National Accelerator Laboratory, Menlo Park, California 94025, United States*

*hemamala@stanford.edu, marina.filip@physics.ox.ac.uk

Table of Contents

1. Materials

General methods: All reagents were purchased from commercial vendors and used as received. Solvents were of reagent grade or higher purity. Powders of (CYS)PbX_2 (X = Cl, Br) were synthesized as previously reported.[1] Abbreviations used: CYS = cysteamine, SeCYS·HCl = selenocysteamine hydrochloride, SeCYS·HBr = selenocysteamine hydrobromide, DMF = *N*,*N*-dimethylformamide, PMMA = polymethyl methacrylate.

Syntheses of SeCYS·HCl and SeCYS·HBr

The SeCYS·HCl ligand was synthesized following a revised reported method.[2] Solid 2,2'-diselanediyldiethanamine dihydrochloride ($H_2N(CH_2)_2Se–Se(CH_2)_2NH_2·2HCl$; 1.20 g, 3.76 mmol) was dissolved in 8 mL of degassed H_2O under a N_2 atmosphere. Then the solution was slowly added to $NaBH_4$ (90.0 mg, 2.38 mmol) in 6 mL of degassed H_2O in an ice bath, resulting in a color change in the solution from yellow to nearly colorless. After stirring for 1 h at room temperature, the solvent was removed using a rotary evaporator at reduced pressure at 55 °C to give a yellow oil. The residue was acidified with 10 mL of hydrogen chloride ethanol solution (cold, ca. 1.25 M), stirring for 30 minutes. The mixture was filtered, and the filtrate was dried under reduced pressure to yield a colorless solid. The SeCYS·HBr was synthesized using a similar procedure as for SeCYS·HCl but using hydrogen bromide ethanol solution (10% – 20%) to acidify the residue oil instead.

Synthesis of (SeCYS)$PbCl_2$

Powders: Solid $PbCl_2$ (50.0 mg, 0.180 mmol) and $Pb(OAc)_2·3H_2O$ (58.0 mg, 0.153 mmol) were combined with 6.0 mL of saturated NaCl (aq.) and 0.5 mL H_2O in a 20 mL scintillation vial. The vial was heated at 90 ºC for 20 minutes with stirring until all solids fully dissolved. Then SeCYS·HCl (58.0 mg, 0.361 mmol) was dissolved with 1.0 mL of saturated NaCl (aq) and 0.5 mL of H_2O at room temperature. The SeCYS·HCl solution was added dropwise into the $PbCl_2$ solution with stirring. The solution turned yellow instantly and a dark red solid precipitated quickly. The mixture was stirred at 90 ºC for 40 minutes. The product was then separated by hot filtration, washed with cold diluted NaCl solution and dried under reduced pressure overnight. Anal. Calcd. for $C_2H_7NSePbCl_2$: C 5.97%, H 1.75%, N 3.48%, Se 19.6%, Pb 51.5%. Found: C 5.92%, H 1.82%, N 3.52%, Se 19%, Pb 52%.

Crystals: Solid $PbCl_2$ (10.0 mg, 0.036 mmol) and $Pb(OAc)_2·3H_2O$ (12.0 mg, 0.031 mmol) were combined with 6.0 mL of saturated NaCl (aq) and 0.5 mL of H_2O in a 20 mL scintillation vial. The mixture was heated at 90 ºC with stirring until all precursors fully dissolved. Then SeCYS·HCl (12.0 mg, 0.072 mmol) was dissolved with 1.0 mL of saturated NaCl (aq) and 0.5 mL of H_2O at room temperature. The two solutions were combined and kept at 90 ºC for 30 minutes. Square dark red crystals formed at the solution-headspace interface (Figure S1).

Synthesis of (SeCYS)$PbBr_2$

Powders: Solid $PbBr_2$ (66.0 mg, 0.180 mmol) and $Pb(OAc)_2·3H_2O$ (58.0 mg, 0.153 mmol) were combined with 6.0 mL of 6-M NaBr (aq) in a 20 mL scintillation vial. The vial was heated at 90

ºC with stirring until all precursors fully dissolved. Then SeCYS·HCl (58.0 mg, 0.361 mmol) was dissolved with 1.0 mL of 6-M NaBr (aq) and 0.5 mL of H_2O at room temperature. The SeCYS·HCl solution was added dropwise into the $PbBr_2$ solution with stirring. The solution turned orange instantly and a black solid precipitated quickly. The mixture was stirred at 90 ºC for 40 minutes. The product was separated by hot filtration, washed with cold diluted NaBr (aq) and dried under reduced pressure overnight. Anal. Calcd. for $C_2H_7NSePbBr_2$: C 4.89%, H 1.44%, N 2.85%, Se 16.1%, Pb: 42.2%. Found: C 5.04%, H 1.33%, N 2.86%, Se 17%, Pb: 44 %.

Synthesis of (SeCYS)$PbCl_{2(1-x)}Br_{2x}$

Solution-state synthesis: The mixed-halide (SeCYS)$PbCl_{2(1-x)}Br_{2x}$ perovskites were prepared using a similar synthesis as for (SeCYS)PbX_2. Solids $PbBr_2$ (66 mg, 0.18 mmol) and $Pb(OAc)_2·3H_2O$ (58 mg, 0.15 mmol) were combined with 6.0 mL of mixed NaCl/NaBr solution (aq) in a 20 mL scintillation vial. The vial was heated at 90 ºC with stirring until all precursors fully dissolved. Then SeCYS·HCl (58 mg) was dissolved with 1.0 mL of the mixed solution at room temperature. The SeCYS·HCl solution was added dropwise into the lead solution with stirring. The mixture was stirred at 90 ºC for 40 minutes. The product was separated by hot filtration and dried under reduced pressure overnight.

Specifically, the perovskite (SeCYS)$PbCl_{1.26}Br_{0.74}$ was prepared from a Cl:Br ratio of 6:1. The perovskite (SeCYS)$PbCl_{0.72}Br_{1.28}$ was prepared from a Cl:Br ratio of 3:1. The perovskite (SeCYS)$PbCl_{0.32}Br_{1.68}$ was prepared from a Cl:Br ratio of 1:1.

Solid-state synthesis: Solid (SeCYS)$PbCl_2$ and (SeCYS)$PbBr_2$ were loaded into a milling bowl with Zirconia balls (ca. 3 g). The lid was sealed with electrical tape. After milling at 800 rpm for 2 h, the powder product was separated using toluene and dried under reduced pressure overnight.

Specifically, the perovskite (SeCYS)$PbCl_{1.5}Br_{0.5}$ was prepared from 48 mg of (SeCYS)$PbCl_2$ and 20 mg of (SeCYS)$PbBr_2$. The perovskite (SeCYS)PbClBr was prepared from 32 mg of (SeCYS)$PbCl_2$ and 39 mg of (SeCYS)$PbBr_2$. The perovskite (SeCYS)$PbCl_{0.5}Br_{1.5}$ was prepared from 16 mg of (SeCYS)$PbCl_2$ and 58 mg of (SeCYS)$PbBr_2$.

Synthesis of $(CYS)_{1-x}(SeCYS)_xPbCl_2$

Solid $PbCl_2$ (84.5 mg, 0.304 mmol) was dissolved in 5.0 mL of DMF at 110 ºC in a 20 mL scintillation vial with stirring, under a N_2 atmosphere. The two ligands CYS and SeCYS·HCl were dissolved in two separate 4 mL scintillation vials with 0.5 mL of DMF with gentle heating at around 60 ºC, and then cooled to room temperature. The two ligand solutions were combined immediately before adding to the $PbCl_2$ solution. Note that the mixing of ligand solutions yielded an off-white cloudy mixture, indicating side reactions between the two ligands. The mixture was stirred at 110 ºC for 30 minutes affording orange to red solids. The product was separated by hot filtration, and dried under reduced pressure overnight.

Note that the SeCYS·HCl ligand decomposed rapidly in DMF above 130 ºC, yielding a deep yellow to black solution. The SeCYS·HCl and CYS ligands react with each other in DMF. Hence, variations of the mixing time of the two ligands and temperature lead to slightly different alloying compositions.

Specifically, the perovskite $(CYS)_{0.86}(SeCYS)_{0.14}PbCl_2$ was prepared with 22.0 mg (0.285 mmol) of CYS and 6.7 mg (0.042 mmol) of SeCYS·HCl. The perovskite $(CYS)_{0.69}(SeCYS)_{0.31}PbCl_2$ was prepared with 17.7 mg (0.229 mmol) of CYS and 12.4 mg (0.077 mmol) of SeCYS·HCl. The perovskite $(CYS)_{0.49}(SeCYS)_{0.51}PbCl_2$ was prepared with 12.5 mg (0.162 mmol) of CYS and 26.0 mg (0.163 mmol) of SeCYS·HCl.

Synthesis of $(CYS)_{1-x}(SeCYS)_xPbBr_2$

Solid $PbBr_2$ (116 mg, 0.316 mmol) was dissolved in 0.5 mL of DMF at 110 ºC in a 4 mL scintillation vial with stirring, under N_2 atmosphere. Two ligands CYS and SeCYS·HBr were dissolved in two separate 4 mL scintillation vials with 0.5 mL of DMF with gentle heating at around 60 ºC and then cooled to room temperature. The two ligand solutions were combined immediately before adding to the $PbBr_2$ solution. Note that the mixing of ligand solutions yielded an off-white cloudy mixture, indicating side reactions between two ligands. The mixture was stirred at 110 ºC for 30 minutes affording orange to red solids. The product was separated by hot filtration, and dried under reduced pressure overnight.

Specifically, the perovskite $(CYS)_{0.76}(SeCYS)_{0.24}PbBr_2$ was prepared with 21.0 mg (0.272 mmol) of CYS and 11.5 mg (0.056 mmol) of SeCYS·HBr. The perovskite $(CYS)_{0.42}(SeCYS)_{0.58}PbBr_2$ was prepared with 15.5 mg (0.201 mmol) of CYS and 24.5 mg (0.120 mmol) of SeCYS·HBr. The perovskite $(CYS)_{0.21}(SeCYS)_{0.79}PbBr_2$ was prepared with 12.5 mg (0.162 mmol) of CYS and 32.6 mg (0.160 mmol) of SeCYS·HBr.

The PXRD patterns indicate that this synthesis contains a small amount of the impurity seen in the synthesis of $(CYS)PbBr_2$[1] even in the SeCYS-rich compositions.

2. Methods

Single-crystal X-ray diffraction (SC-XRD)

Crystals of $(SeCYS)PbCl_2$ were kept in a minimal amount of mother liquor and transferred to a glass slide containing Paratone-N® oil shortly after synthesis. A small fragment of a large crystal was used to avoid twin boundaries. Crystals were coated with Paratone-N® oil, attached to a Kapton® loop, and transferred to a Bruker D8 Venture diffractometer equipped with a Photon 100 CMOS detector. The mounted crystal was enveloped by a flow of N_2 and did not show significant decay during data collection. Frames were collected using ω and φ scans and the unit-cell parameters were refined against all data. Data were integrated and corrected using SAINT V8.38A for Lorentz and polarization effects.[3] The absorption corrections were performed using SADABS-2016/2. Space-group assignments were based upon systematic absences, *E*-statistics, agreement factors for equivalent reflections and successful refinement of the structures. The structure was

solved using the intrinsic phasing method implemented in SHELXT-2014.[4] The solution was refined against all data using the SHELXL-2018/3 software package[5] and OLEX2[6]. The anion site was refined as a mixture of Cl and Se. The freely refined occupancies of Cl (0.655) and Se (0.345) are close to the theoretical values (0.667 and 0.333 for Cl and Se, respectively). The residual electron density calculated by OLEX2 shows that most differences are located close to the anion site, which indicates disorder in the structure. To account for the disordered organic component, a solvent mask function in OLEX2 was applied to improve the solution.[7] A solvent mask was calculated, and 144 electrons were found per unit cell. This is consistent with the presence of one C_2NH_7 per formula unit, which accounts for 156 electrons per unit cell. Although the SC-XRD solution does not show SeCYS, the presence of SeCYS in the perovskite A-site cavity could be independently verified through numerous methods:

1) By dissolving the perovskite and showing that the solution-state NMR spectrum is that of SeCYS (Figures S18, S19).
2) Using ^{77}Se solid-state NMR, we see that the SeCYS molecule coordinates to the Pb via the terminal Se^- in the solid perovskite samples.
3) The ^{13}C solid-state NMR also clearly shows that the chemical shifts of the *β*-C and α-C in SeCYS (Figure S16) in the solid perovskite.
4) Using XPS, we see that the binding energy of Se corresponds to that of a metal selenide instead of a selenol (–SeH) group, indicating the formation of Pb–Se bonds (Figure S3).
5) Using Raman spectroscopy, we find that the higher-energy peaks (> 200 cm^{-1}) can be assigned to bond vibrations and twists characteristic to SeCYS. By integrating the Raman peaks we can further determine the ratios of the *trans*:*gauche* rotational isomer to be 8.6 and 6.3 for (SeCYS)$PbCl_2$ and (SeCYS)$PbBr_2$ within the A-site cavity (Figure 2).
6) The PXRD of the bulk perovskite matches the simulated PXRD from the SC-XRD solution showing us that the structure is that of the bulk material.

Therefore, we can conclude that SeCYS, with the Se coordinated to the Pb, is in the A-site cavity of the perovskite, with a preference for adopting the *trans* rotamer.

Powder X-ray diffraction (PXRD)

PXRD data were collected using a Bruker D8 Advance Diffractometer equipped with a Cu source ($K\alpha_1$ = 1.54060 Å, $K\alpha_2$ = 1.54443 Å, $K\alpha_2/K\alpha_1$ = 0.5), fixed divergence slits with a nickel filter and a LYNXEYE 1D detector. The instrument was operated in a Bragg-Brentano geometry with a step size of 0.02°. Fine power samples were dispersed in toluene and transferred to a clean glass slide. The measurements were conducted under ambient atmosphere. Simulated powder patterns were calculated directly from the crystallographic information files (CIFs) generated from PDF fitting using the Mercury software. The cell parameters (*a*, *c* axes and volumes) of the alloyed perovskites were obtained using La Bail fitting in the GSAS-II software.[8]

Elemental analysis

Inductively couple plasma mass spectrometry (ICP-MS) data were collected at the Stanford University Environmental Measurements Facility using a Thermo XSeries II ICP-Mass Spectrometer. Powders of (L)PbX_2 (ca. 3 mg) were dissolved in 10 mL of 1.4% aqueous HNO_3 followed by filtration through glass filter paper. This stock solution was diluted with 1.4% aqueous

HNO_3 to prepare a series of samples for ICP-MS analysis of Pb and Se. The C, H, and N analyses were performed by Midwest Microlab (Indianapolis, IN).

Pair distribution function (PDF) analysis

High-energy X-ray ($\lambda = 0.2115$ Å) total scattering data suitable for PDF analysis were collected at beamline 11-ID-B, Advanced Photon Source, at Argonne National Laboratory. The 2D scattering images were reduced to 1D data within GSAS-II.[8] PDFs were extracted from the 1D scattering data up to $Q_{max} = 23$ Å^{-1} within xPDFsuite.[9] Structure models for the perovskites were refined within PDFgui.[10] First, we refined the structures by assuming that the Ch/X ligands occupy the same coordinates, similar to our previous PDF analyses of (CYS)PbX_2 (X = Cl, Br), which were also used for DFT calculations.[1] These CIFs are named "(L)PbX_2 PDF models for DFT". Considering the possible different bond lengths between Pb–X and Pb–Ch, as explained in the main text, we further optimized the PDF models by allowing separate atomic coordinates for the Se and X sites and considering different ranges of data for refinement (long range: 2 – 30 Å; short range: 2 – 12 Å). These files are named as: (L)PbX_2_long-range_PDF or (L)PbX_2_short-range_PDF.

X-ray photoelectron spectroscopy (XPS)

XPS data were measured using a PHI Versaprobe 3, equipped with a focused Ar ion gun (FIG) and electron gun. Finely ground powders of (SeCYS)PbX_2 (X = Cl, Br) were prepared on electrical tape (2 mm × 2 mm). Survey scans were collected with a pass energy of 224 eV from 1100 eV to 0 eV. High-resolution scans were collected with a pass energy of 55 eV for C 1s, Pb 4f, Se 3p, Cl 2p, and Br 3d signals. To minimize charging effects, the samples were neutralized using a FIG and electron gun. The high-resolution scans were calibrated using C 1s as the reference peak. The molar elemental ratios were estimated by integrating peak areas from the high-resolution scans.

Raman spectroscopy

Raman spectra were collected using a Renishaw RM1000 Raman microscope equipped with a 633 nm laser for (CYS)$PbCl_2$ and (SeCYS)$PbCl_2$, and a HORIBA Scientific LabRAM HR Evolution spectrometer equipped with a 785 nm laser for (SeCYS)$PbBr_2$. The samples were ground into fine powder and loaded on a clean glass substrate. Repeated scans showed no signs of decomposition by oxidation or by the laser over the course of 10 minutes.

Diffuse reflectance spectroscopy

Diffuse reflectance measurements were conducted using a Shimadzu UV-2600 spectrometer equipped with an integrating sphere. The spectra were collected with a reflective backing of compressed $BaSO_4$ mixed with the samples. The spectra were converted to pseudo-absorbance spectra using the Kubelka–Munk transformation.[11]

Photoluminescence spectroscopy

Low-temperature steady-state emission spectra were measured using a Horiba Jobin-Yvon Spex Nanolog fluorimeter equipped with a 450-W xenon lamp, R928P detector (for visible signals from

400 nm to 850 nm), H10300B-75 IR detector (for infrared signals from 950 nm to 1500 nm), and Symphony Near-IR CCD detector (for infrared signals from 800 nm to 1500 nm). The excitation wavelength was between 410 – 460 nm. The powder samples were prepared by mixing a suspension of the perovskites with a solution of PMMA in toluene. This slurry was then allowed to dry at room temperature and cooled to 80 K in a Janis ST-100 cryostat.

Thermogravimetric analyses

Thermogravimetric analyses (TGA) were conducted with a Netzsch TG 209 F1 Libra Thermo-Microbalance at a heating rate of 1 °C/minute from room temperature to 500 ºC under N_2 flow, using ca. 10 – 20 mg of the samples in alumina crucibles. An empty alumina crucible was used as correction before the sample measurement. The decomposition temperature (T_d) is defined as the temperature corresponding to 5% mass loss.

Photostability test

Powders of the organochalcogenide-halide perovskites (ca. 50 mg) were spread on glass slides (in air) and illuminated under an infinityPV ISOSun solar similar calibrated to 1 sun intensity (AM1.5 G, 0.1 $W \cdot cm^{-2}$ simulated). The samples reached a temperature of 40 °C during illumination. The samples were monitored by PXRD at different time intervals (Figure S30).

Solution-state proton nuclear magnetic resonance (^{1}H NMR) spectroscopy

^{1}H NMR spectra were recorded using a 400 MHz Varian NMR spectrometer. Solid SeCYS·HCl was dissolved in DCl solution in D_2O (35 wt.%) or MeOD for analysis by NMR. The perovskite sample (ca. 40 mg) was mixed with 1.2 mL of the DCl solution in D_2O (35 wt.%) and allowed to sit for 1 h in the dark. The solution was then filtered, and the filtrate was analyzed by NMR within 30 minutes.

Figure S16 shows that the dissolved (SeCYS)PbX_2 (X = Cl and Br) exhibit the same proton signals as those of the precursor ligand SeCYS·HCl. Notably, we observed a broad low-field triplet (intensity ratio of 1:2:1), which is attributed to ammonium protons. The splitting and intensity ratio suggest that the ammonium protons are coupling with the two protons on the adjacent C (β-C). Although the ammonium protons should also have the ^{14}N–^{1}H coupling (1:1:1 triplet), this may be hidden due to the peak broadness. Usually, the ammonium protons are not resolved in protic solvent due to isotope exchange. The possible intramolecular hydrogen bonding and highly acidic conditions might slow down this exchange. Then based on the chemical shifts and multiplicity, we assign the high-field sextet and triplet to be protons on the β-C and α-C, respectively. The side bands from ^{77}Se–^{1}H coupling are not observed due to spectral overlap.

Solid-state nuclear magnetic resonance (ssNMR) spectroscopy

All the samples were packed in 4 mm OD ZrO_2 rotors and all the NMR spectra were collected at 11.75 T on a Bruker Avance 500 spectrometer, using a double resonance H/X Bruker probe at room temperature (~298 K).

^{207}Pb ssNMR: All ^{207}Pb NMR data were acquired under static (non-spinning) conditions, using a Hahn-echo pulse sequence (90°−τ−180°−τ−acquire) with an echo delay of 20.85 μs. A recycle delay of 2 s was applied. For all the samples, a variable offset cumulative spectra (VOCS) approach was applied with 16 steps and a 35 kHz (for 11.75 T) transmitter stepping frequency across the spectral range to get a complete and undistorted spectrum. The sub-spectra were added using the skyline projection method. Two-dimensional ^{207}Pb–^{207}Pb exchange spectroscopy (EXSY) NMR spectra were acquired at 11.75 T by using a mixing time of 2 ms. Due to the wide ^{207}Pb spectra, reaching a complete 2D EXSY spectrum covering all offsets is unrealistic for the lead samples on this instrument. Thus, quasi-2D EXSY spectra of (CYS)$PbCl_2$, (SeCYS)$PbCl_2$, and (SeCYS)$PbBr_2$ were obtained at offsets of −720, −60, and 240 ppm, respectively. A total of 64 slices were acquired in the indirect dimension using a 2 μs increment and 2 s recycle delay, with 1520 transients per slice. Due to the very short T_2 of (SeCYS)$PbCl_2$, the quasi-2D EXSY spectrum could not be acquired for this sample. All ^{207}Pb NMR spectra were referenced to 1.0 M $Pb(NO_3)_2$ in D_2O by setting δ (^{207}Pb) = −2990 ppm at room temperature (~298 K).

^{77} Se ssNMR: ^{77}Se NMR data were collected under magic-angle spinning (MAS) conditions using a spinning rate of 10 kHz. All Se-contained samples were measured by applying ^{77}Se{^{1}H} cross-polarization (CP) pulse sequence with a recycle delay of 2 s and a contact time of 3 ms. All ^{77}Se NMR spectra were referenced to saturated H_2SeO_3 solution by setting δ(^{77}Se) = 1300 ppm at room temperature (~298 K).

^{13}C ssNMR: All carbon spectra were acquired under a spinning rate of 10 kHz. A ^{13}C{^{1}H} cross-polarization (CP) pulse sequence was used to obtain ^{13}C NMR spectra with a recycle delay of 2 s and contact time of 3 ms. All carbon chemical shifts were referenced externally to adamantane at 38.48 ppm at room temperature (~298 K).

Calculations of the distributions of Pb local coordination environments

The organochalcogenide-halide perovskites can be viewed as close analogs to the mixed-halide perovskite with a halide alloying ratio = 1:2. However, the major difference lies in the zwitterions that connect the A site and X site, which adds an additional restriction to the distributions of the chalcogenide. Hence, the binomial distributions used in the ideal mixed-halide perovskites no longer hold true in the case of organochalcogenide-halide perovskites. We designed a Python algorithm to simulate the anion distributions and calculate the Pb coordination environments, which is available in the Supporting Information.

Basic Assumptions: (1) The perovskite structure is cubic and undistorted (idealized octahedra and no octahedral tilting); (2) the zwitterions are built by the connection of A and X sites; (3) one A site randomly chooses one of the closest, available X sites; (4) the same X site can only connect to one A site.

Stepwise Description of the Algorithm: (1) Build a superlattice of the perovskite structure and create lists of the coordinates of the A, Pb, and X sites; (2) iterate over all the A sites to randomly switch one X anion into a chalcogenide based on the basic assumptions mentioned above; (3) iterate over all the Pb atoms to identify the local coordination; (4) output the distributions of local coordination environments. See the illustration in Figure 3 (manuscript).

Computational methodology

All the density functional theory (DFT) calculations in this manuscript have been carried out with the Quantum Espresso package[12], using the same computational setup as described in the previous work on (CYS)PbX_2.[1] The lattice parameters of (SeCYS)PbX_2 (X = Cl, Br) and the Wyckoff positions of Pb, Se, and X, were taken from the crystallographic information files generated by PDF measurements. The structural models of (SeCYS)PbX_2 and $CsPb(SeH)X_2$ were constructed using the same approach as described in the SI of our previous work.[1]

The conduction and valence band edges of (SeCYS)PbX_2 exhibit a noticeable Rashba-Dresselhaus-type splitting, which is likely an artifact of the ordering of the chalcogenide and halide in the model structures. This effect is less prominent in (CYS)PbX_2, as expected given the smaller atomic number of S. To correct for this artifact in the calculation of the effective masses, we first average the spin-split conduction and valence band edges before calculating their curvatures. In Table S3, we list the effective masses of all $LPbX_2$ (L = CYS, SeCYS) compounds and related model structures computed on the same footing. Values for (CYS)PbX_2 are slightly smaller than those reported in the previous work,[1] where only the singly occupied band edges were used to calculate the second derivative.

The band structure plots display an anisotropic band dispersion, flatter along the Γ to K direction, and more dispersive along other directions (e.g., Γ to A or M) for both (CYS)PbX_2 and (SeCYS)PbX_2 perovskites. In order to understand the origin of such anisotropy, we considered structural models of $CsPbCl_3$ and the hypothetical $CsPb(SeH)_3$ based on the (SeCYS)PbX_2 structures. The lattice constants were kept fixed, and the anionic sites were populated with halide/chalcogenide to makeup the compositions of the two perovskites. In the case of $CsPb(SeH)_3$, only the Cs atoms and the H atoms attached to Se were relaxed. We then calculated and compared the band structures of $CsPbCl_3$, $CsPb(SeH)_3$ and $CsPb(SeH)Cl_2$ as shown in Figure 5 and Figure S14 (for the S analogs).

In these cases, the Pb within a given octahedron is bonded to six X/Se atoms. The square modulus of the electron wave function corresponding to the valence band maximum is shown via contour plots for three different Pb–Cl/Se bonding planes in Figure S15. The displayed contour constitutes the sum of the squared wave function of both the degenerate orbitals at the VBM. Among the different perovskites, we focused on the Se/Cl case as this has the largest standard deviation (among the three eigen directions) in its effective masses, shown in Table S3.

3. Supplementary Data

Table S1. Crystallographic data for (SeCYS)$PbCl_2$

Compound	(SeCYS)$PbCl_2$
Empirical formula	$C_2H_7NCl_{1.96}PbSe_{1.04}$
Formula weight (g/mol)	403.75
Temperature (K)	100
Crystal system	trigonal
Space group	*R*-3*c*
a (Å)	8.1207(7)
b (Å)	8.1207(7)
c (Å)	19.883(2)
α (°)	90
γ (°)	120
Volume (Å^3)	1135.5(2)
Z	6
Density, calc. (g/cm^3)	3.543
Absorption coeff. (mm^{-1})	27.859
F(000)	1060.0
Crystal size (mm^3)	0.15 × 0.10 × 0.10
Radiation	Mo Kα (λ = 0.71073 Å)
2θ range (°)	7.098 to 54.124
Index ranges	$-10 \le h \le 10$, $-9 \le k \le 10$, $-25 \le l \le 25$
Reflections collected/unique	3222/289
Completeness to θ_{max}	1.00
Max. and min. transmission	0.4301/0.3261
Data/restraints/parameters	289/0/9
Goodness-of-fit on F^2	1.252
Final *R* indices [$I > 2\sigma(I)$][a]	R_1 = 0.0687 wR_2 = 0.1706
R indices (all data)[a]	R_1 = 0.0768 wR_2 = 0.1745
Largest diff. peak/hole (e/Å^3)	5.17/−5.54

[a] $R_1 = \Sigma||F_o| - |F_c||/\Sigma|F_o|$, w$R_2 = [\Sigma w(F_o^2 - F_c^2)^2/\Sigma(F_o^2)^2]^{1/2}$

Table S2. Structural parameters from refinements against long-range PDF data (2 – 30 Å)

Compound	$(SeCYS)PbCl_2$	$(SeCYS)PbBr_2$
Temperature (K)	300	300
Space group	*R-3c*	*R-3c*
a (Å)	8.124(3)	8.351(5)
c (Å)	20.182(13)	20.694(24)
delta-1	2.36(6)	2.14(8)
s-ratio (r_{cut}=3.55Å)	0.93(17)	0.81(4)
Atomic coordinates	Pb: (0,0,0)	Pb: (0, 0, 0)
	Cl: (0.565(8), 0.565(8), 0.25)	Br: (0.564(5), 0.564(5), 0.25)
	Se: (0.591(9), 0.591(9), 0.25)	Se: (0.597(11), 0.597(11), 0.25)
	virtual K atom: (0, 0, 0.25)	virtual K atom: (0, 0, 0.25)
U_{iso}	Pb: 0.0249(11)	Pb: 0.0347(14)
	Cl: 0.083(16)	Br: 0.076(4)
	Se: 0.131(31)	Se: 0.113(30)
	virtual K atom: 0.624(65)	virtual K atom: 0.619(96)
R_w	14.3%	16.9%

Table S3. Structural parameters from refinements against short-range PDF data (2 – 12 Å)

Compound	$(SeCYS)PbCl_2$	$(SeCYS)PbBr_2$
Temperature (K)	300	300
Space group	*R*-3*c*	*R*-3*c*
a (Å)	8.122 (3)	8.354(6)
c (Å)	20.198(13)	20.684(28)
delta-1	2.33(4)	2.17(5)
s-ratio (r_{cut}=3.55Å)	0. 91(4)	0.80(3)
Atomic coordinates	Pb: (0,0,0)	Pb: (0, 0, 0)
	Cl: (0.567(9), 0.567(9), 0.25)	Br: (0.564(5), 0.564(5), 0.25)
	Se: (0.590(11), 0.590(11), 0.25)	Se: (0.597(12), 0.597(12), 0.25)
	virtual K atom: (0, 0, 0.25)	virtual K atom: (0, 0, 0.25)
U_{iso}	Pb: 0.0237 (9)	Pb: 0.0353(22)
	Cl: 0.083(18)	Br: 0.072(9)
	Se: 0.122(29)	Se: 0.129(35)
	virtual K atom: 0.635(63)	virtual K atom: 0.589(91)
R_w	12.4%	14.0%

Table S4. Calculated band gaps and orbital contributions for orthorhombic (experimental[13]) and rhombohedral (hypothetical, with the lattice parameters of (SeCYS)PbX_2) $CsPbX_3$, (SeCYS)PbX_2 and (CYS)PbX_2, with X = Cl and Br. The values of (CYS)PbX_2 are reproduced from the previous work[1] for ease of comparison. The VBM and CBM contributions (in fraction) of different elements are evaluated at the Γ-point.

Structures	Band gap (eV)	VBM contributions			CBM contributions		
		Se/S	X	Pb	Se/S	X	Pb
Orthorhombic $CsPbCl_3$	1.00	0.00	0.67	0.33	0.00	0.09	0.92
Orthorhombic $CsPbBr_3$	0.72	0.00	0.71	0.29	0.00	0.08	0.92
Rhombohedral $CsPbCl_3$	1.59	0.00	0.75	0.25	0.00	0.08	0.92
Rhombohedral $CsPbBr_3$	1.00	0.00	0.74	0.26	0.00	0.08	0.92
(SeCYS)$PbCl_2$	0.53	0.67	0.12	0.22	0.04	0.05	0.91
(SeCYS)$PbBr_2$	0.41	0.60	0.18	0.23	0.03	0.05	0.92
(CYS)$PbCl_2$	0.80	0.58	0.19	0.22	0.08	0.08	0.85
(CYS)$PbBr_2$	0.65	0.52	0.25	0.22	0.03	0.05	0.92
Trans $CsPb(SeH)Cl_2$	0.57	0.61	0.15	0.24	0.03	0.05	0.92
Trans $CsPb(SeH)Br_2$	0.48	0.55	0.21	0.24	0.03	0.06	0.91
Cis and *Trans* $CsPb(SeH)Cl_2$	0.70	0.52	0.21	0.27	0.02	0.06	0.92
Cis and *Trans* $CsPb(SeH)Br_2$	0.54	0.47	0.27	0.26	0.02	0.06	0.92

Table S5. Calculated effective masses for orthorhombic (experimental[13]) and rhombohedral (hypothetical, with the lattice parameters of (SeCYS)PbX_2) $CsPbX_3$, (SeCYS)PbX_2 and (CYS)PbX_2, with X = Cl and Br. The average effective mass values are the harmonic mean over the three eigenvalues of the effective mass tensor.

Structures	Hole Effective Mass (VBM)					Electron Effective Mass (CBM)				
	m^*_{h11}	m^*_{h22}	m^*_{h33}	$\langle m^*_h \rangle$	Std. Dev.	m^*_{e11}	m^*_{e22}	m^*_{e33}	$\langle m^*_e \rangle$	Std. Dev.
Orthorhombic $CsPbCl_3$	0.172	0.192	0.200	0.187	0.012	0.215	0.212	0.188	0.204	0.012
Orthorhombic $CsPbBr_3$	0.139	0.154	0.165	0.152	0.011	0.163	0.160	0.139	0.153	0.011
Rhombohedral $CsPbCl_3$	0.320	0.320	0.354	0.331	0.016	0.328	0.327	0.325	0.327	0.001
Rhombohedral $CsPbBr_3$	0.205	0.205	0.232	0.213	0.013	0.207	0.203	0.202	0.204	0.002
(SeCYS)$PbCl_2$	0.069	0.381	0.452	0.155	0.221	0.257	0.232	0.117	0.179	0.065
(SeCYS)$PbBr_2$	0.069	0.221	0.254	0.131	0.095	0.163	0.151	0.102	0.133	0.027
(CYS)$PbCl_2$	0.111	0.414	0.473	0.222	0.194	0.273	0.265	0.198	0.240	0.034
(CYS)$PbBr_2$	0.116	0.232	0.273	0.181	0.071	0.186	0.173	0.170	0.176	0.007
trans $CsPb(SeH)Cl_2$	0.063	0.337	0.406	0.141	0.196	0.262	0.229	0.096	0.161	0.079
trans $CsPb(SeH)Br_2$	0.068	0.217	0.243	0.128	0.091	0.171	0.158	0.094	0.131	0.035
cis and *trans* $CsPb(SeH)Cl_2$	0.088	0.340	0.449	0.181	0.187	0.281	0.239	0.125	0.191	0.070
cis and *trans* $CsPb(SeH)Br_2$	0.084	0.205	0.251	0.144	0.079	0.179	0.161	0.108	0.142	0.031

Table S6. Room-temperature crystallographic data for the organochalcogenide-halide perovskites and their chalcogenide/halide alloys

Compositions	Space group	***a*** (Å)	***c*** (Å)	***V*** (Å^3)	Method
(CYS)$PbCl_2$	*R*-3*c*	8.028(5)	19.94(3)	1113(2)	PDF
(CYS)$PbBr_2$	*R*-3*c*	8.260(7)	20.41(4)	1206(3)	PDF
(SeCYS)$PbCl_2$	*R*-3*c*	8.130(4)	20.17(2)	1155(2)	PDF
(SeCYS)$PbBr_2$	*R*-3*c*	8.359(7)	20.67(3)	1251(3)	PDF
(SeCYS)$PbCl_{1.26}Br_{0.74}$	*R*-3*c*	8.192(2)	20.31(1)	1180(1)	PXRD
(SeCYS)$PbCl_{0.76}Br_{1.24}$	*R*-3*c*	8.247(1)	20.44(1)	1204(1)	PXRD
(SeCYS)$PbCl_{0.32}Br_{1.68}$	*R*-3*c*	8.303(3)	20.58(1)	1229(1)	PXRD
$(CYS)_{0.86}(SeCYS)_{0.14}PbCl_2$	*R*-3*c*	8.040(2)	19.95(1)	1117(1)	PXRD
$(CYS)_{0.69}(SeCYS)_{0.31}PbCl_2$	*R*-3*c*	8.059(2)	19.99(1)	1124(1)	PXRD
$(CYS)_{0.49}(SeCYS)_{0.51}PbCl_2$	*R*-3*c*	8.078(1)	20.02(2)	1131(2)	PXRD
$(CYS)_{0.76}(SeCYS)_{0.24}PbBr_2$	*R*-3*c*	8.261(2)	20.49(2)	1211(2)	PXRD
$(CYS)_{0.42}(SeCYS)_{0.58}PbBr_2$	*R*-3*c*	8.292(1)	20.59(2)	1226(2)	PXRD
$(CYS)_{0.21}(SeCYS)_{0.79}PbBr_2$	*R*-3*c*	8.314(2)	20.63(1)	1235(1)	PXRD

Table S7. Experimental Raman modes and tentative assignments

Perovskite			Assignment
$(CYS)PbCl_2$	$(SeCYS)PbCl_2$	$(SeCYS)PbBr_2$	
648 w	553 w	553 w	$\nu(C–Ch)_G$
738 m	657 s	655 s	$\nu(C–Ch)_T$
805 w	733 w	732 m	$r(CH_2)_{Ch}$
	897 sh	891 sh	$\nu(C–C–N) + r(CH_2)_N$
918 m	911 m	906 m	
996 w	995 w	989 w	$r(CH_2)_{Ch} + r(CH_2)_N$
1057 w	1034 w	1031 w	$\nu(C–N) + t(CH_2)_{Ch}$
1123 w	1121 w	1117 w	$t(CH_2)_N + t(NH_3)$
1264 vs	1227 vs	1231 vs	$wag(CH_2)_{Ch}$
1314 w	1314 w	1316 w	$wag(CH_2)_N$
1369 w	1367 w	1368 w	$t(CH_2)_N + t(NH_3)$
1421 w	1419 w	1421 w	$\delta(CH_2)_{Ch}$
1452 sh	1451 sh	1450 sh	$\delta(CH_2)_N$
1481 w	1478 w	1473 w	
1565 w	1564 w	1561 w	$\delta(NH_3)$

Abbreviations: T: *trans*; G: *gauche*; m: middle; w: weak; s: strong; vs: very strong; sh: shoulder. ν: stretching; δ: deformation; r: rocking; wag: wagging; t: twisting. $(CH_2)_{Ch}$ and $(CH_2)_N$ refer to the methylene groups adjacent to the Ch (chalcogenide) and N atoms, respectively. The assignments were mostly based on the reported experimental and calculated Raman modes of the zwitterionic cysteamine ligand.[14]

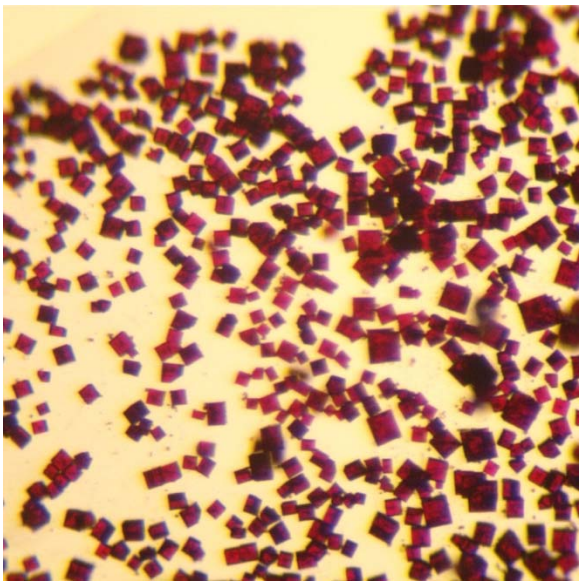

Figure S1. Photos of (SeCYS)$PbCl_2$ crystals. Most of the crystals are visibly twinned into four domains. The SC-XRD experiments were performed using a fragment of the crystals. The (SeCYS)$PbBr_2$ crystals were too small for measurement through SC-XRD.

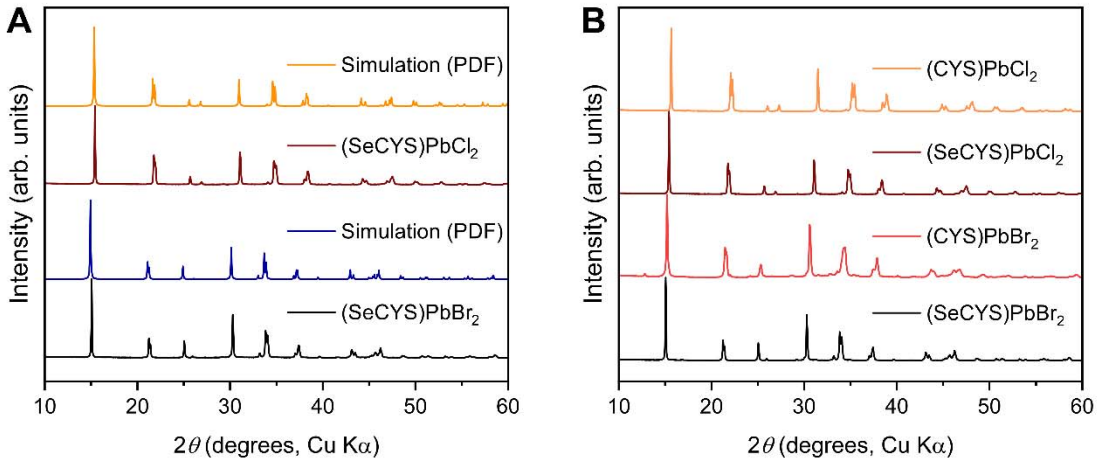

Figure S2. (A) Experimental powder X-ray diffraction patterns of (SeCYS)PbX_2 (dark red line for X = Cl and black line for X = Br), in agreement with the simulated patterns from the PDF models. (B) Comparison of the PXRD patterns of the four organochalcogenide-halide perovskites.

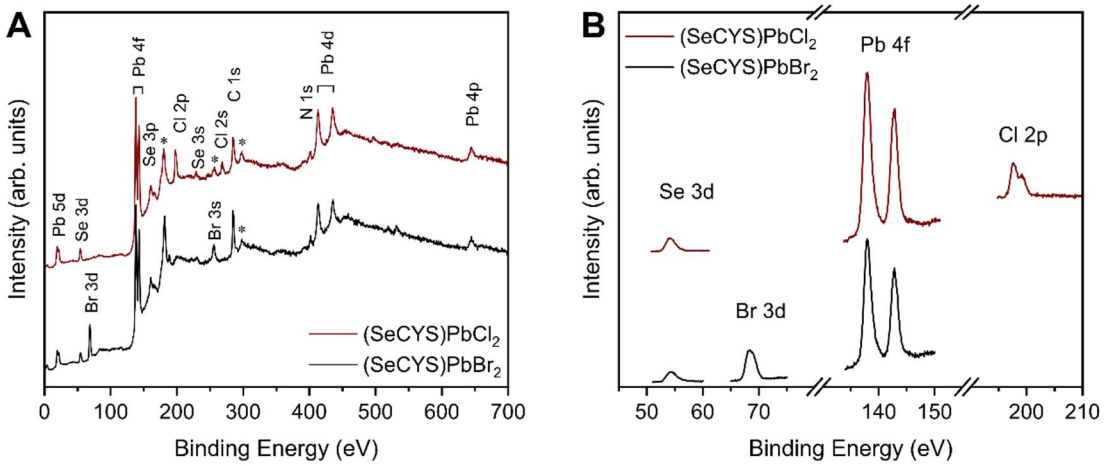

Figure S3. (A) XPS survey spectra of (SeCYS)PbX_2 (X = Cl, Br) powders, ranging from 0 to 700 eV. The asterisks indicate the Se LMM peaks. (B) High-resolution XPS scans for Se 3d, Pb 4f, Cl 2p, and Br 3d.

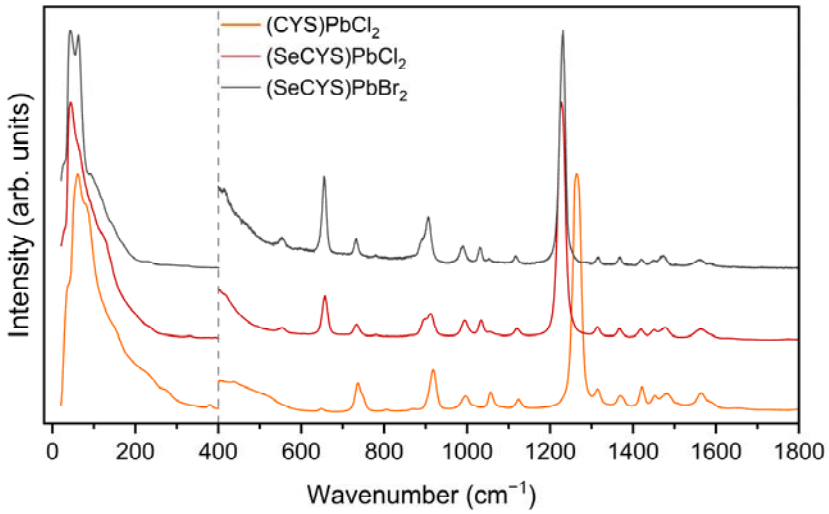

Figure S4. Experimental Raman spectra of (L)PbX_2 (L = CYS, SeCYS). The 400 – 1800 cm^{-1} range is magnified ca. 10 times to show the ligand Raman signals.

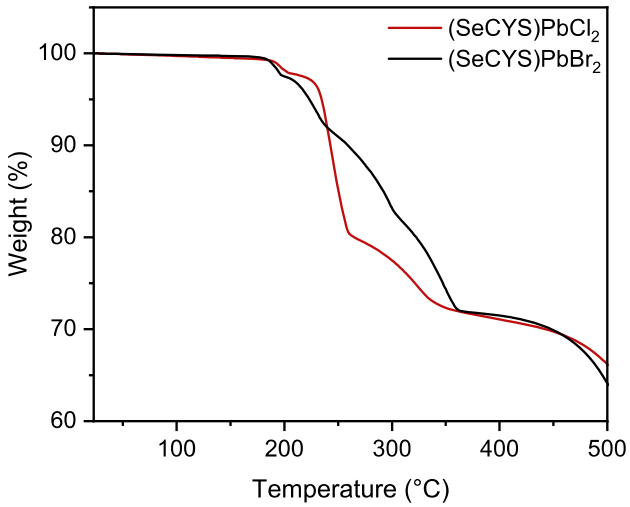

Figure S5. Thermogravimetric analysis of (SeCYS)PbX_2 at a scan rate of 1 °C/minute, measuring from room temperature to 500 °C.

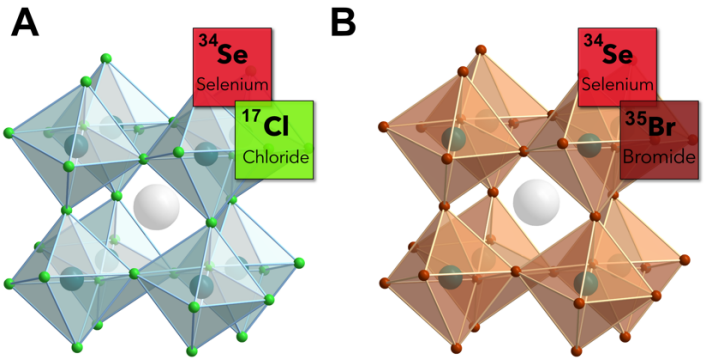

Figure S6. Structures of (A) (SeCYS)$PbCl_2$ and (B) (SeCYS)$PbBr_2$ in the *R*-3*c* space group (room temperature), derived from pair distribution function (PDF) analysis with the disordered organoammonium tail of SeCYS represented by a gray sphere. Turquoise, green, brown, gray spheres represent Pb, Cl/Se, Br/Se, and K(proxy) atoms, respectively.

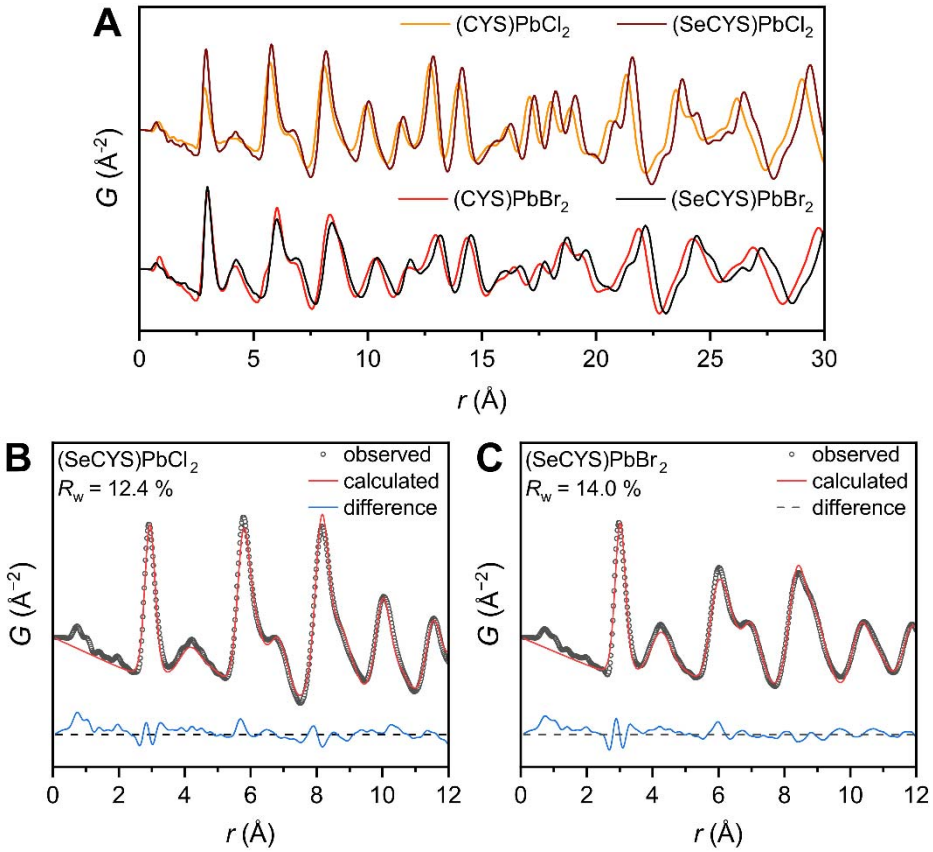

Figure S7. (A) PDF comparison of the four organochalcogenide-halide perovskites. PDF fitting of (B) (SeCYS)$PbCl_2$ and (C) (SeCYS)$PbBr_2$ on a short range (2 – 12 Å).

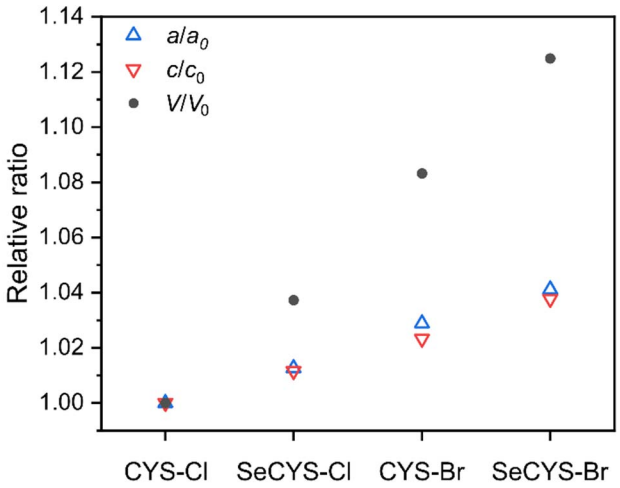

Figure S8. Comparison of relative cell parameters of the four organochalcogenide-halide perovskites. The parameters were all obtained from room-temperature PDF refinements and the ratios were calculated with respect to the cell parameters of (CYS)$PbCl_2$.

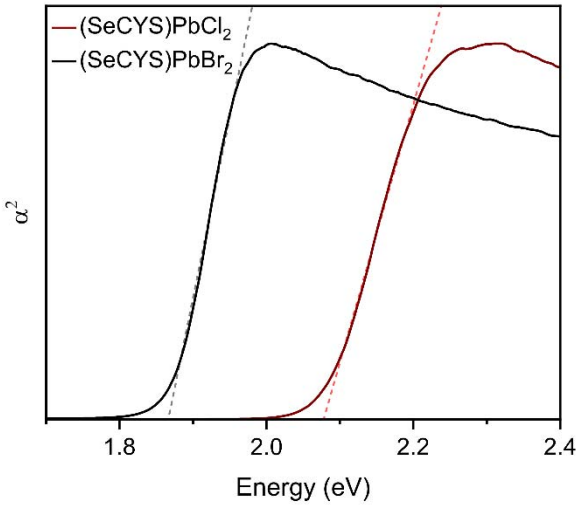

Figure S9. The direct-gap Tauc plot of α^2 vs. E to determine the optical bandgaps of (SeCYS)PbX_2. Fits to the linear portion of the plot give the direct bandgap values of 2.07 eV and 1.86 eV for X = Cl and Br, respectively.

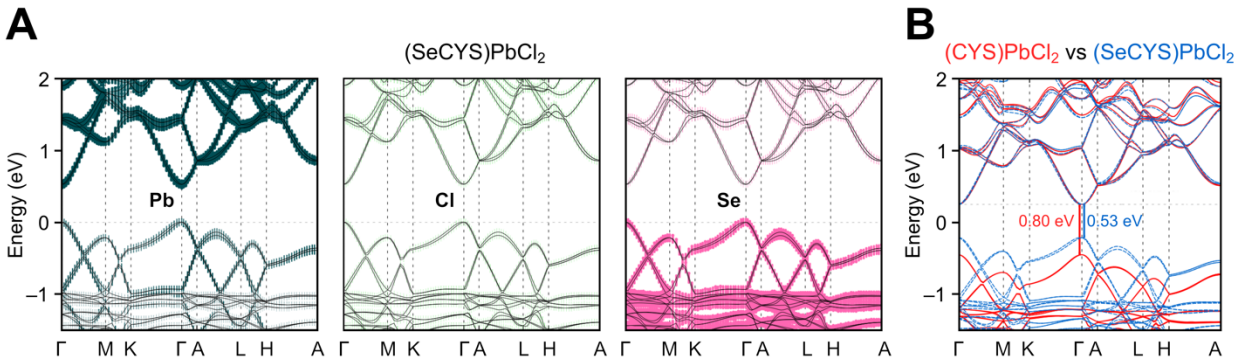

Figure S10. (A) Band structures of (SeCYS)$PbCl_2$. The Pb, Cl, and Se orbitals that contribute to the bands are depicted as turquoise, green, and magenta dots, with the dot size proportional to the orbital contribution. (B) Comparison of the band structures of (CYS)$PbCl_2$ vs. (SeCYS)$PbCl_2$, where the conduction band minima have been arbitrarily aligned.

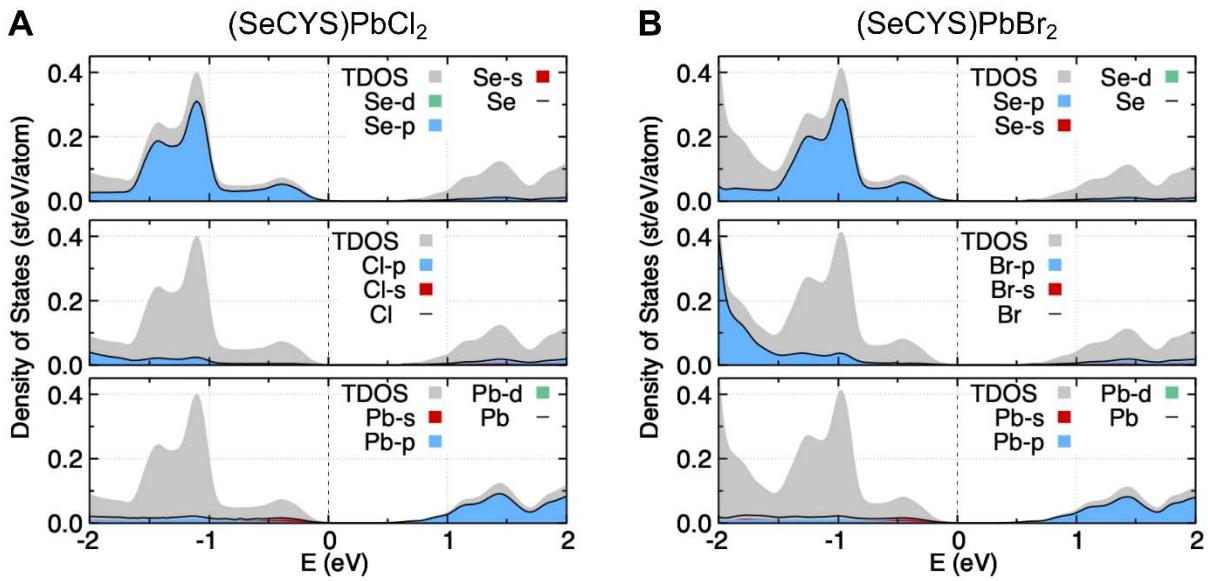

Figure S11. Total density of states (TDOS) and atom projected density of states (PDOS) calculated for (A) (SeCYS)$PbCl_2$, and (B) (SeCYS)$PbBr_2$.

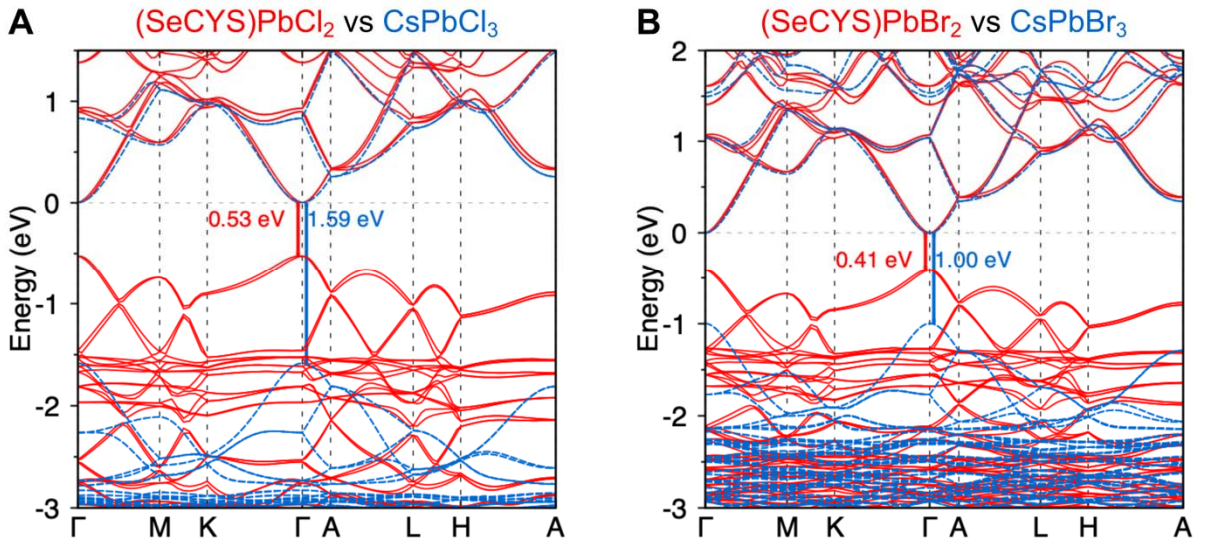

Figure S12. Comparison of the band structures of (A) (SeCYS)$PbCl_2$ and hypothetical $CsPbCl_3$, and (B) (SeCYS)$PbBr_2$ and hypothetical $CsPbBr_3$, all in the *R*-3*c* space group. The conduction-band minima have been arbitrarily aligned, for ease of comparison.

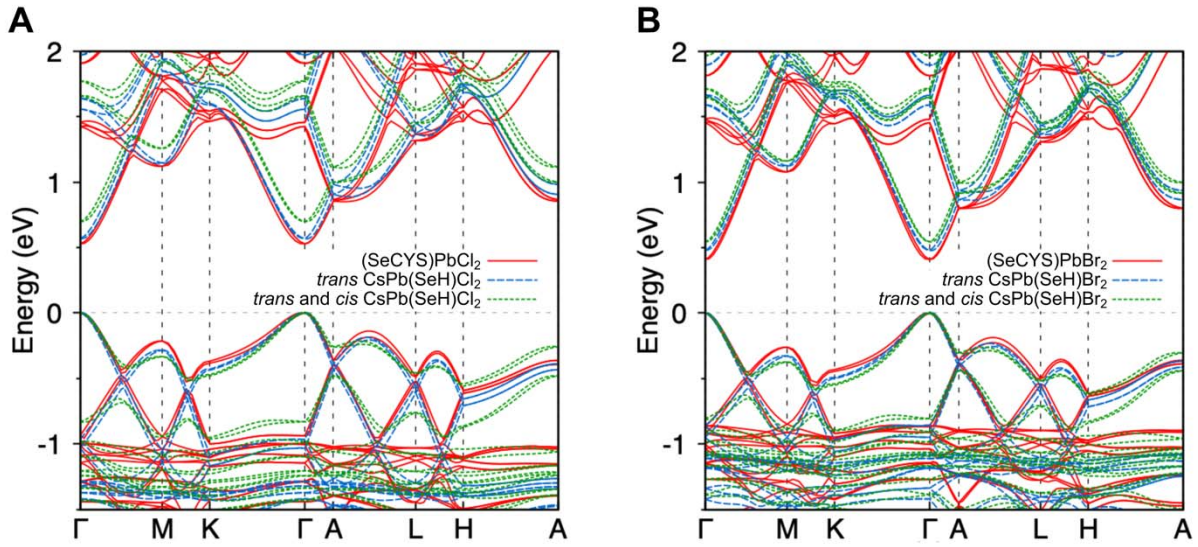

Figure S13. Band structures of (SeCYS)PbX_2 (red solid) and $CsPb(SeH)X_2$ model structures with *trans* (blue dashed) and both *cis* and *trans* (green dashed) ordering of Se atoms for (A) X = Cl and (B) X = Br in a rhombohedral unit cell. Band structures are aligned to the valence band maxima for clarity.

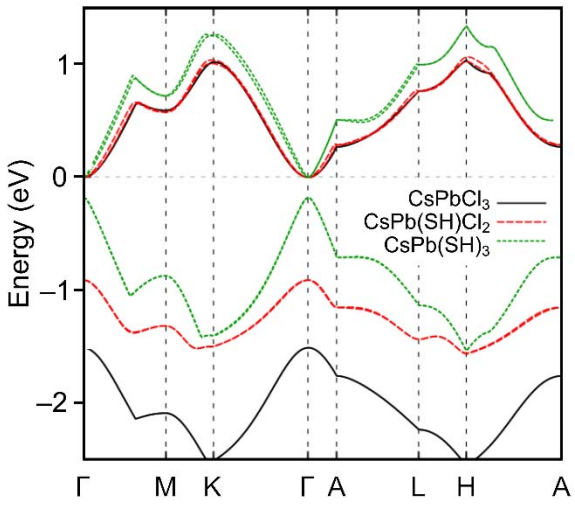

Figure S14. Comparison of the band structures of $CsPbCl_3$, *trans* $CsPb(SH)Cl_2$, and $CsPb(SH)_3$, all in the *R*-3*c* space group. The conduction band minima have been arbitrarily aligned.

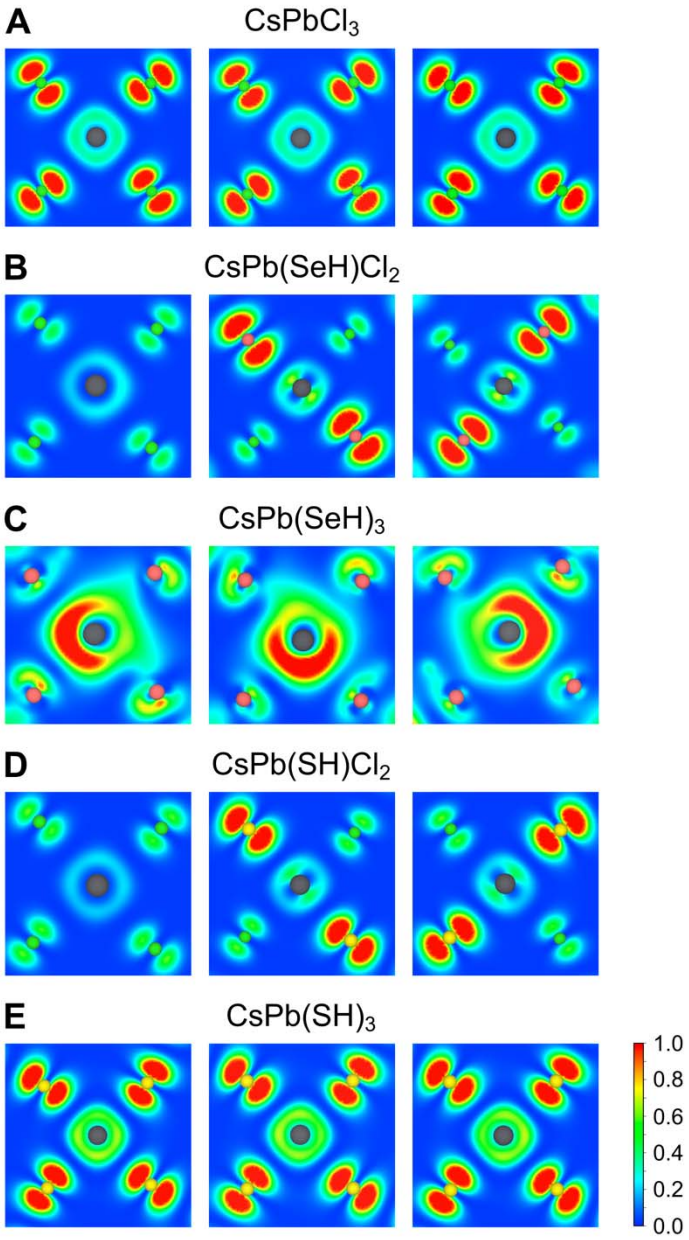

Figure S15. The square modulus of the electronic wave function corresponding to the valence band maximum state of (A) $CsPbCl_3$, (B) *trans* $CsPb(SeH)Cl_2$, (C) $CsPb(SeH)_3$, (D) *trans* $CsPb(SH)Cl_2$, and (E) $CsPb(SH)_3$ at the valence band maximum (Γ point) along three orthogonal cross sections of the Pb octahedra in the same order (from left, middle, to right). The Pb, Cl, S and Se atoms are colored black, green, yellow, and orange, respectively. The anisotropic ligand environment (Se/Cl or S/Cl) leads to asymmetric Pb orbitals.

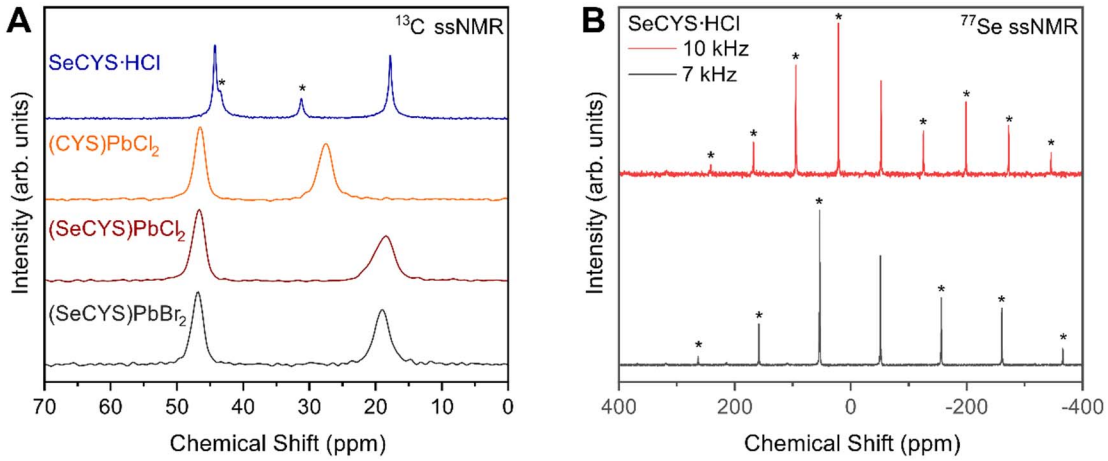

Figure S16. (A) ^{13}C ssNMR spectra of SeCYS·HCl, (CYS)PbCl$_2$, (SeCYS)PbCl$_2$, and (SeCYS)PbBr$_2$ with magic-angle spinning (MAS) frequency of 10 kHz. The asterisks indicate an impurity in SeCYS·HCl (likely due to oxidation by O_2). (B) ^{77}Se ssNMR spectra of SeCYS·HCl with MAS frequency of 10 kHz and 7 kHz at 11.7 T. The asterisks indicate spinning sidebands.

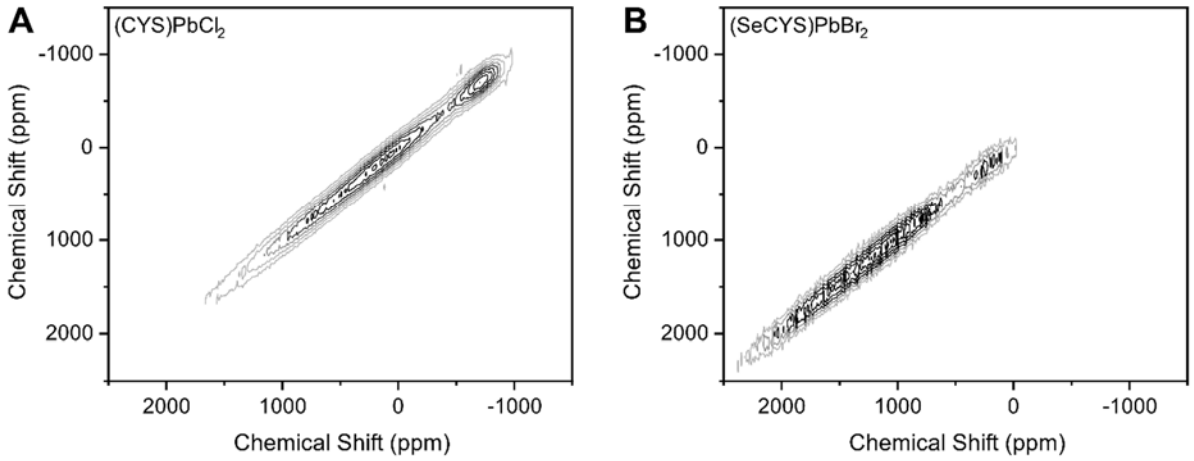

Figure S17. Two-dimensional ^{207}Pb EXSY NMR spectra of (CYS)PbCl$_2$ and (SeCYS)PbBr$_2$ obtained using 2 ms mixing time. Spectra were acquired at 11.75 T under non-spinning conditions at ambient temperature.

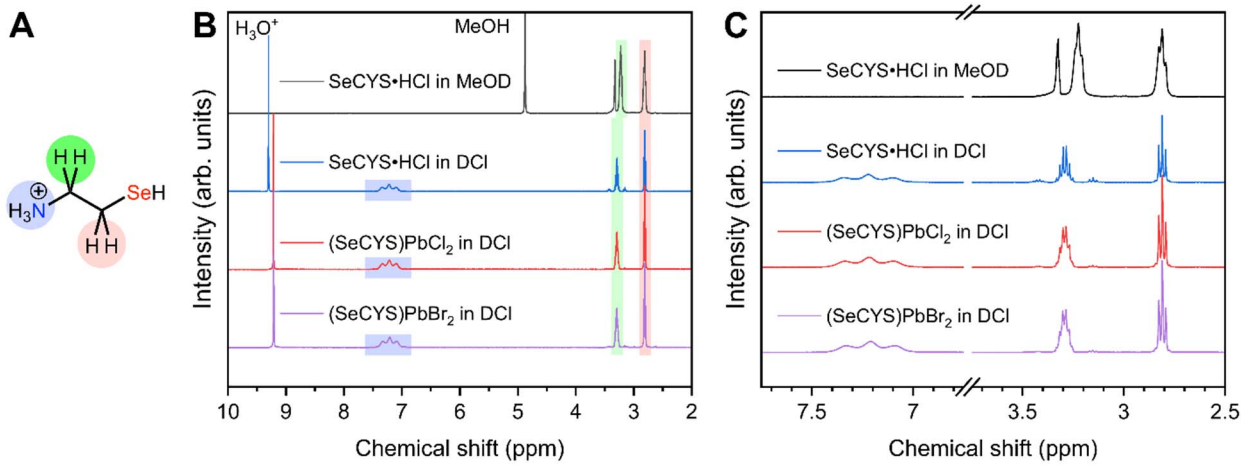

Figure S18. (A) The molecular structure of the selenocysteammonium cation. The hydrogen in the ammonium group, β-C, and α-C are colored in blue, green, and pink, respectively. (B) The solution-state ^{1}H-NMR spectra of selenocysteamine hydrochloride, and (SeCYS)$PbCl_2$ and (SeCYS)$PbBr_2$ dissolved in MeOD or DCl solution in D_2O (35 wt. %). The same color code is used as in (A) to distinguish different hydrogen peaks. (C) A magnified view of the spectra in (B).

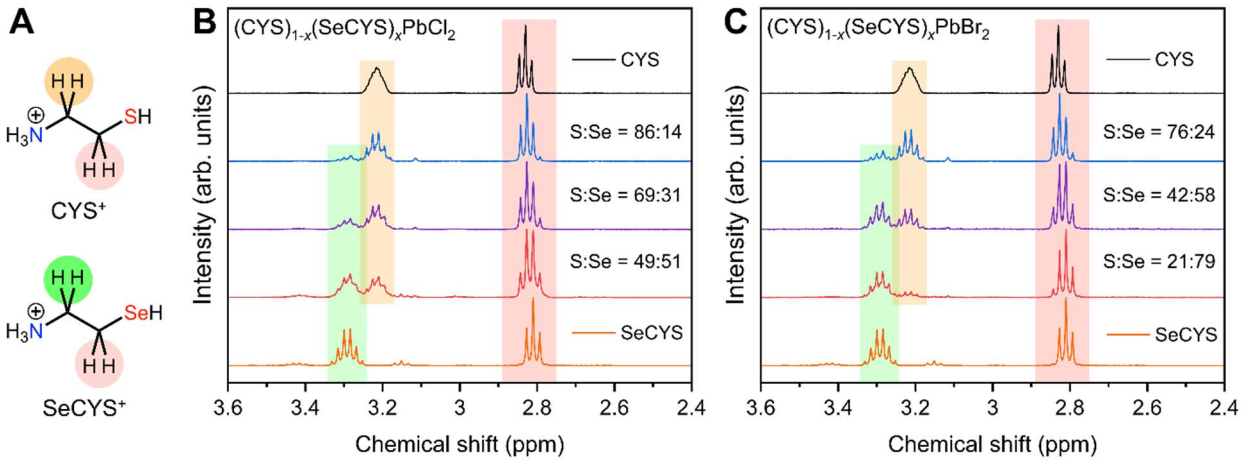

Figure S19. (A) The molecular structures of the selenocysteammonium cation and cysteammonium cation. The CYS^+ hydrogen in the β-C and α-C are colored in orange and pink, respectively. The $SeCYS^+$ hydrogen in the β-C and α-C are colored in green and pink, respectively. (B) The solution-state ^{1}H-NMR spectra of $(CYS)_{1-x}(SeCYS)_xPbCl_2$ dissolved in DCl solution in D_2O (35 wt. %). The same color code is used as in (A) to distinguish different hydrogen peaks. (C) The solution-state ^{1}H-NMR spectra of $(CYS)_{1-x}(SeCYS)_xPbBr_2$ dissolved in DCl solution in D_2O (35 wt. %). The same color code is used as in (A) to distinguish different hydrogen peaks. The CYS/SeCYS ratios are estimated by integrating the signals from the β-C hydrogens.

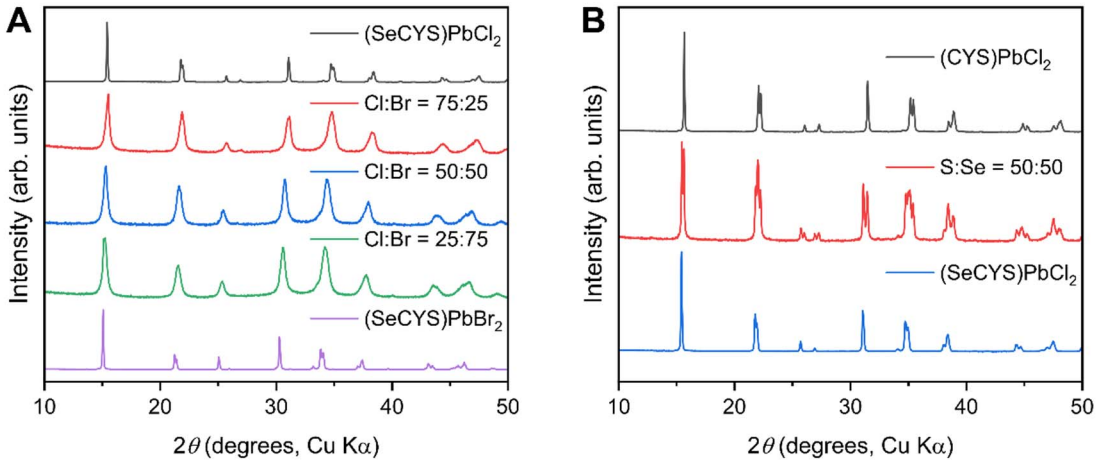

Figure S20. (A) Experimental powder X-ray diffraction patterns of (SeCYS)$PbCl_2$, (SeCYS)$PbCl_{2(1-x)}Br_{2x}$ synthesized by ball milling (showing alloying of the halides), and (SeCYS)$PbBr_2$. (B) Experimental powder X-ray diffraction patterns of (CYS)$PbCl_2$, a 1:1 mixture of (CYS)$PbCl_2$ and (SeCYS)$PbCl_2$ after ball milling (showing a mixture of precursors instead of alloying of the organochalcogenides), and (SeCYS)$PbCl_2$.

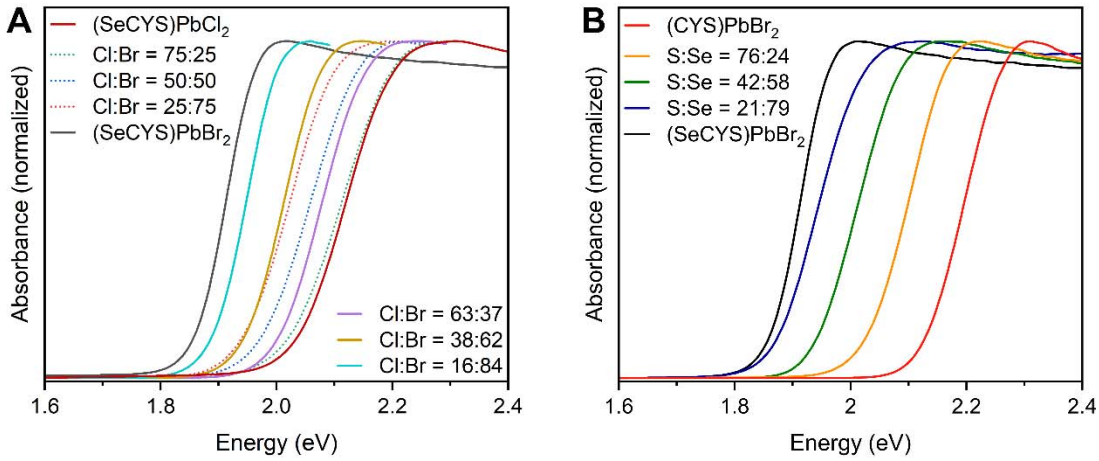

Figure S21. (A) Diffuse reflectance spectra of (SeCYS)$PbBr_2$, (SeCYS)$PbCl_{2(1-x)}Br_{2x}$ synthesized by ball milling (dashed line) and by solution-state synthesis (solid line), and (SeCYS)$PbCl_2$. The Cl:Br ratios of samples synthesized in solution were determined by ICP-MS and the Cl:Br ratios of the samples synthesized through mechanical milling correspond directly to the precursor stoichiometry. The slight differences in the steepness of the absorption onsets may depend on particle size, as we have previously noted.[15] (B) Diffuse reflectance spectra of (CYS)$PbBr_2$, $(CYS)_{1-x}(SeCYS)_xPbBr_2$, and (SeCYS)$PbBr_2$. The S:Se ratios were determined by ^{1}H NMR of the dissolved product.

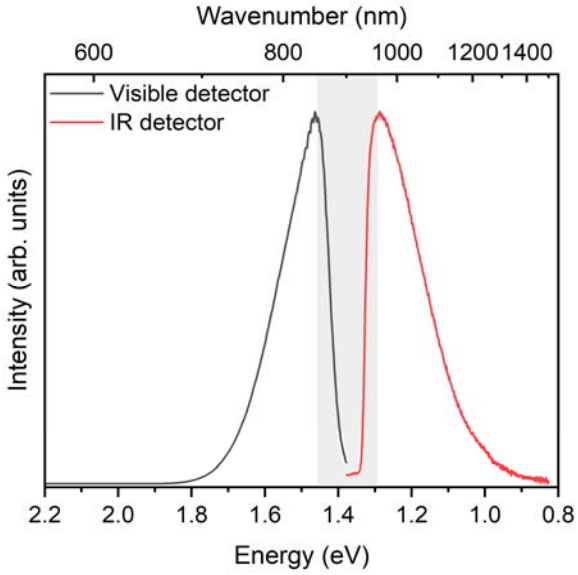

Figure S22. Photoluminescence spectra of (SeCYS)$PbBr_2$ at 80 K collected by a R928P detector (black line; for visible signals), and by an H10300B-75 IR detector (red line; for IR signals). Both spectra are normalized to the maximum intensity. The shaded area indicates the energy window outside the two detectors, where the measured intensity is not reliable.

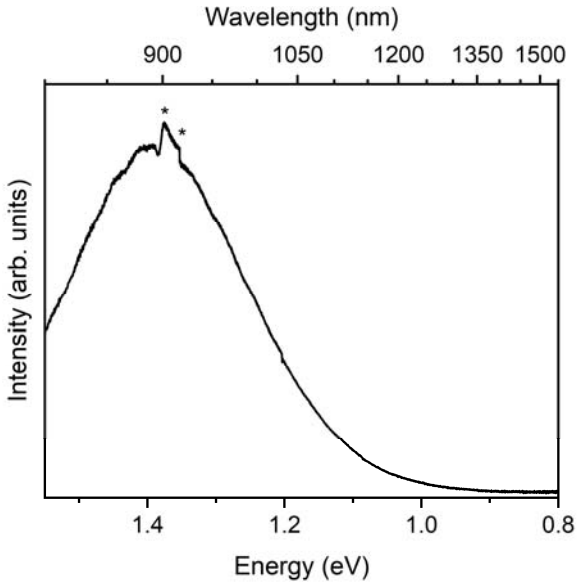

Figure S23. Photoluminescence spectra of (SeCYS)$PbBr_2$ at 80 K collected by a Symphony Near-IR CCD detector. The emission maximum is estimated to be at 1.4 eV. The asterisks indicate experimental artifacts, possibly from the detector correction.

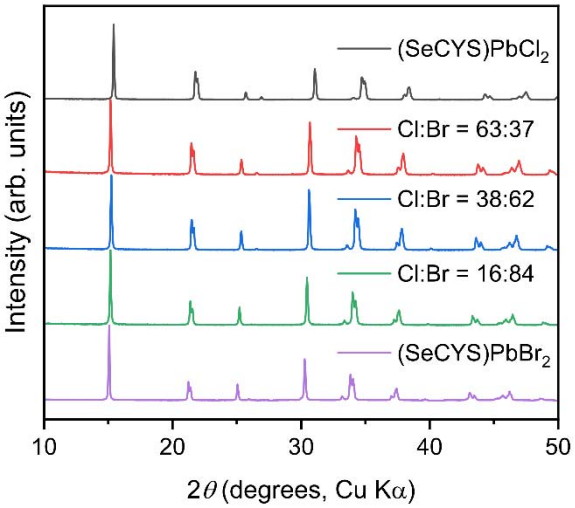

Figure S24. Experimental powder X-ray diffraction patterns of (SeCYS)$PbCl_2$, (SeCYS)$PbCl_{2(1-x)}Br_{2x}$, and (SeCYS)$PbBr_2$.

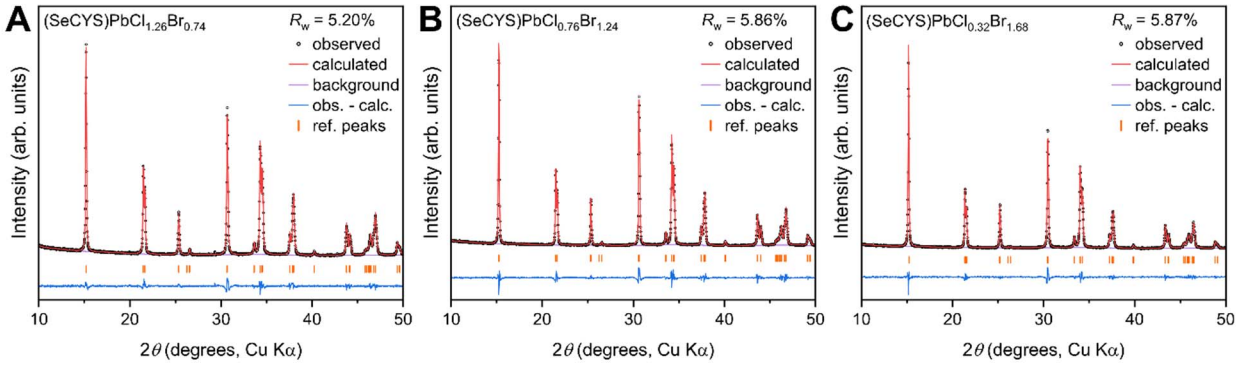

Figure S25. Le Bail refinements for the powder X-ray diffraction patterns of the compositions (A) (SeCYS)$PbCl_{1.26}Br_{0.74}$, (B) (SeCYS)$PbCl_{0.76}Br_{1.24}$, and (C) (SeCYS)$PbCl_{0.32}Br_{1.68}$. Reflection positions are shown as orange tick marks.

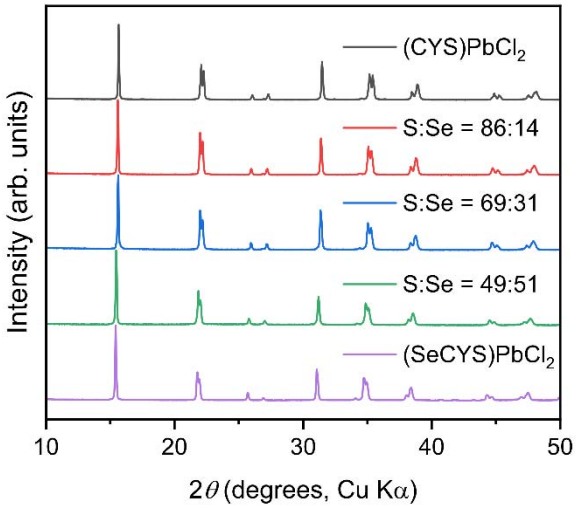

Figure S26. Experimental powder X-ray diffraction patterns of $(CYS)PbCl_2$, $(CYS)_{1-x}(SeCYS)_xPbCl_2$, and $(SeCYS)PbCl_2$.

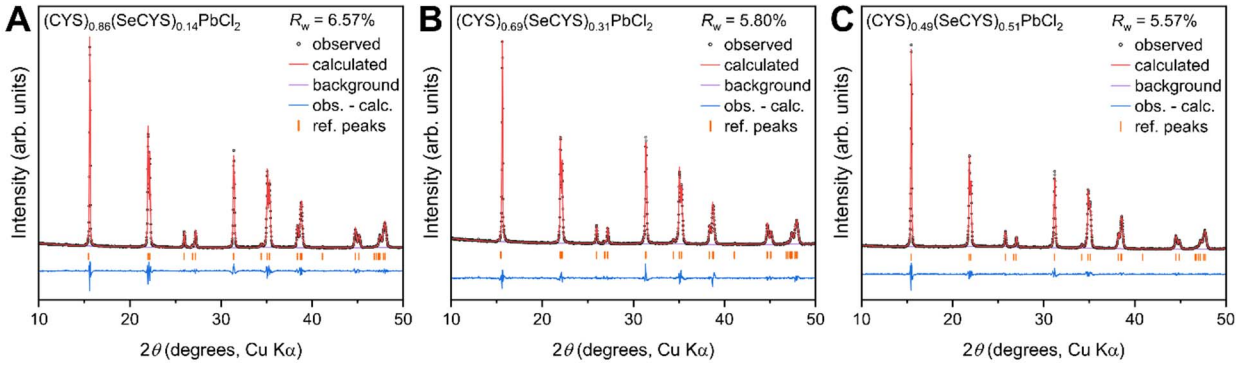

Figure S27. Le Bail refinements for the powder X-ray diffraction patterns of the compositions (A) $(CYS)_{0.86}(SeCYS)_{0.14}PbCl_2$, (B) $(CYS)_{0.69}(SeCYS)_{0.31}PbCl_2$, and (C) $(CYS)_{0.49}(SeCYS)_{0.51}PbCl_2$. Reflection positions are shown as orange tick marks. The CYS:SeCYS ratios were determined by ^{1}H NMR in solution.

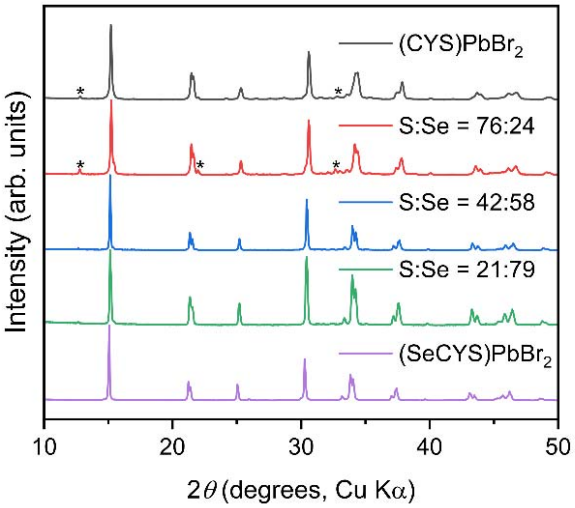

Figure S28. Experimental powder X-ray diffraction patterns of $(CYS)PbCl_2$, $(CYS)_{1-x}(SeCYS)_xPbBr_2$, and $(SeCYS)PbBr_2$. Asterisks denote the impurity described in the previous report on $(CYS)PbBr_2$.[1]

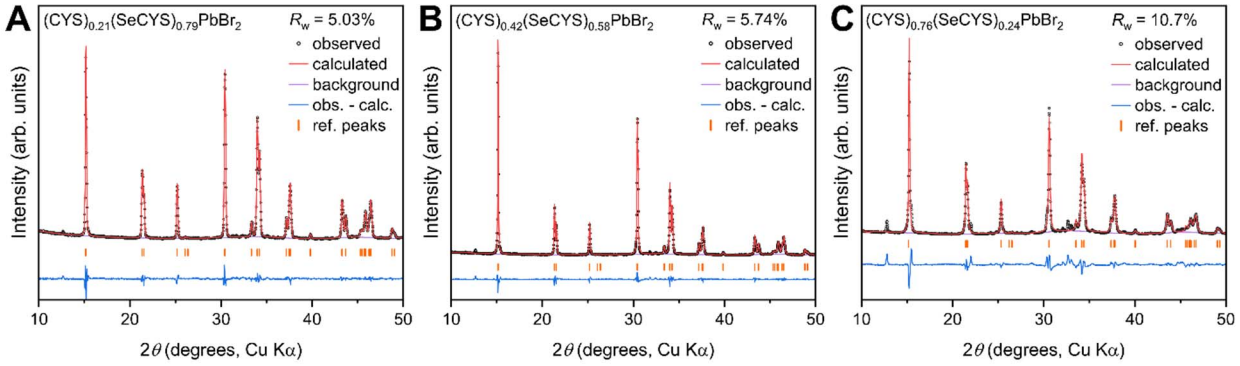

Figure S29. Le Bail refinements for the powder X-ray diffraction patterns of the compositions (A) $(CYS)_{0.21}(SeCYS)_{0.79}PbBr_2$, (B) $(CYS)_{0.42}(SeCYS)_{0.58}PbBr_2$, and (C) $(CYS)_{0.76}(SeCYS)_{0.24}PbBr_2$. Reflection positions are shown as orange tick marks. The synthesis of CYS-rich perovskites contains more of the heterostructure impurity as discussed in the synthesis section and previous report on $(CYS)PbBr_2$.[1] The CYS:SeCYS ratios were determined by ^1H NMR in solution.

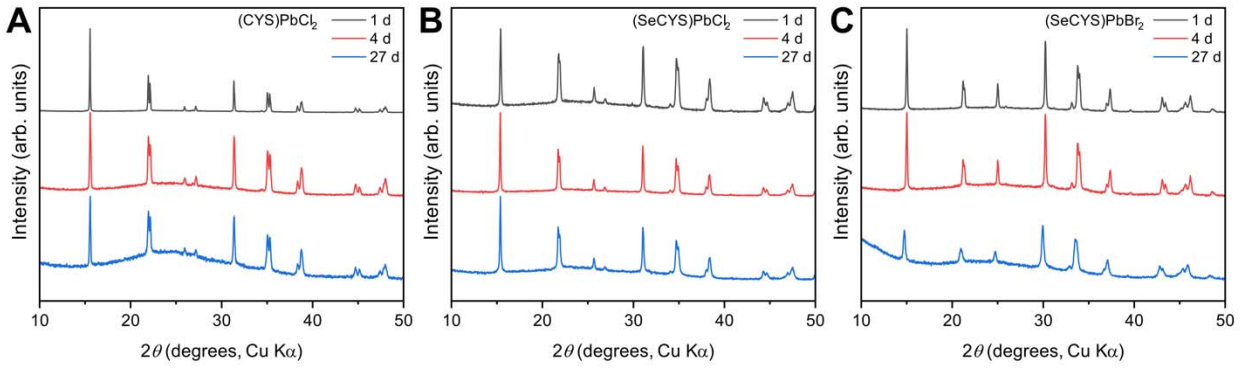

Figure S30. Experimental powder X-ray diffraction patterns of (A) (CYS)$PbCl_2$, (B) (SeCYS)$PbCl_2$, and (C) (SeCYS)$PbBr_2$ under 1-sun illumination, in air at 40 °C, after different time intervals.

References

(1) Li, J.; Chen, Z.; Saha, S.; Utterback, J. K.; Aubrey, M. L.; Yuan, R.; Weaver, H. L.; Ginsberg, N. S.; Chapman, K. W.; Filip, M. R.; Karunadasa, H. I. Zwitterions in 3D Perovskites: Organosulfide-Halide Perovskites. *J. Am. Chem. Soc.* **2022**, *144* (49), 22403–22408. https://doi.org/10.1021/jacs.2c09382.

(2) Klayman, D. L. The Synthesis of Aminoethyl-Substituted Selenium Compounds. *J. Org. Chem.* **1965**, *30* (7), 2454–2456. https://doi.org/10.1021/jo01018a504.

(3) Bruker, APEX. SAINT and SADABS Bruker AXS Inc. *Madison, Wisconsin, USA* **2007**.

(4) Sheldrick, G. M. SHELXT – Integrated Space-Group and Crystal-Structure Determination. *Acta Cryst. A* **2015**, *71* (1), 3–8. https://doi.org/10.1107/S2053273314026370.

(5) Sheldrick, G. M. Crystal Structure Refinement with SHELXL. *Acta Cryst. C* **2015**, *71* (1), 3–8. https://doi.org/10.1107/S2053229614024218.

(6) Dolomanov, O. V.; Bourhis, L. J.; Gildea, R. J.; Howard, J. a. K.; Puschmann, H. OLEX2: A Complete Structure Solution, Refinement and Analysis Program. *J. Appl. Cryst.* **2009**, *42* (2), 339–341. https://doi.org/10.1107/S0021889808042726.

(7) van der Sluis, P.; Spek, A. L. BYPASS: An Effective Method for the Refinement of Crystal Structures Containing Disordered Solvent Regions. *Acta Cryst. A* **1990**, *46* (3), 194–201. https://doi.org/10.1107/S0108767389011189.

(8) Toby, B. H.; Von Dreele, R. B. GSAS-II: The Genesis of a Modern Open-Source All Purpose Crystallography Software Package. *J. Appl. Cryst.* **2013**, *46* (2), 544–549. https://doi.org/10.1107/S0021889813003531.

(9) Yang, X.; Juhas, P.; Farrow, C. L.; Billinge, S. J. L. xPDFsuite: An End-to-End Software Solution for High Throughput Pair Distribution Function Transformation, Visualization and Analysis. **2014**, 1–4. https://doi.org/10.48550/arXiv.1402.3163.

(10) Farrow, C. L.; Juhas, P.; Liu, J. W.; Bryndin, D.; Božin, E. S.; Bloch, J.; Proffen, T.; Billinge, S. J. L. PDFfit2 and PDFgui: Computer Programs for Studying Nanostructure in Crystals. *J. Phys.: Condens. Matter* **2007**, *19* (33), 335219. https://doi.org/10.1088/0953-8984/19/33/335219.

(11) Kubelka, P.; Munk, F. Z. Ein Beitrag Zur Optik Der Farbanstriche. *Zeitschrift fur Technische Physik* **1931**, *12*, 593–601.

(12) Giannozzi, P.; Andreussi, O.; Brumme, T.; Bunau, O.; Nardelli, M. B.; Calandra, M.; Car, R.; Cavazzoni, C.; Ceresoli, D.; Cococcioni, M.; Colonna, N.; Carnimeo, I.; Corso, A. D.; Gironcoli, S. de; Delugas, P.; DiStasio, R. A.; Ferretti, A.; Floris, A.; Fratesi, G.; Fugallo, G.; Gebauer, R.; Gerstmann, U.; Giustino, F.; Gorni, T.; Jia, J.; Kawamura, M.; Ko, H.-Y.; Kokalj, A.; Küçükbenli, E.; Lazzeri, M.; Marsili, M.; Marzari, N.; Mauri, F.; Nguyen, N. L.; Nguyen, H.-V.; Otero-de-la-Roza, A.; Paulatto, L.; Poncé, S.; Rocca, D.; Sabatini, R.; Santra, B.; Schlipf, M.; Seitsonen, A. P.; Smogunov, A.; Timrov, I.; Thonhauser, T.; Umari, P.; Vast, N.; Wu, X.; Baroni, S. Advanced Capabilities for Materials Modelling with Quantum ESPRESSO. *J. Phys.: Condens. Matter* **2017**, *29* (46), 465901. https://doi.org/10.1088/1361-648X/aa8f79.

(13) Linaburg, M. R.; McClure, E. T.; Majher, J. D.; Woodward, P. M. $Cs_{1-x}Rb_xPbCl_3$ and $Cs_{1-x}Rb_xPbBr_3$ Solid Solutions: Understanding Octahedral Tilting in Lead Halide Perovskites. *Chem. Mater.* **2017**, *29* (8), 3507–3514. https://doi.org/10.1021/acs.chemmater.6b05372.

(14) Riauba, L.; Niaura, G.; Eicher-Lorka, O.; Butkus, E. A Study of Cysteamine Ionization in Solution by Raman Spectroscopy and Theoretical Modeling. *J. Phys. Chem. A* **2006**, *110* (50), 13394–13404. https://doi.org/10.1021/jp063816g.

(15) Lindquist, K. P.; Mack, S. A.; Slavney, A. H.; Leppert, L.; Gold-Parker, A.; Stebbins, J. F.; Salleo, A.; Toney, M. F.; Neaton, J. B.; Karunadasa, H. I. Tuning the Bandgap of $Cs_2AgBiBr_6$ through Dilute Tin Alloying. *Chem. Sci.* **2019**, *10* (45), 10620–10628. https://doi.org/10.1039/C9SC02581B.